Ionic Wind Devices Prepared by a 3D Printer

S. Kanazawa[1], W. Imagawa[1], S. Matsunari[1], S. Akamine[1], R. Ichiki[1], and K. Kanazawa[2]
[1]Department of Electrical and Electronic Engineering, Oita University, Japan
[2]Department of Aerospace Systems Engineering, Sojo University, Japan

Abstract—Corona discharges are widely used in many industrial applications such as gas cleaning, particle precipitation, and gas flow control. Essentially, the corona discharge apparatus comprises metallic electrodes and supporting insulators. Typically, the insulators are made of plastic, ceramics, or glass. As such, limitations exist in the design and fabrication of the apparatus. We have previously introduced 3D printing technology in the development of non-thermal plasma reactors. In this study, we investigate the manufacture of ionic wind devices (IWDs) based on a DC corona discharge. Except for the metal electrodes, the IWDs were prepared using a 3D printer. The corona discharge electrode is a needle-to-mesh configuration. We evaluated the performance of the IWDs with respect to the gas flow velocity and its spatial distribution. Moreover, using a multi-device array, we examined the effect of array configurations comprising three IWDs. An advantage of the array is that it is possible to increase the ionic wind velocity and broadly control the air flow distribution.

Keywords—3D printer, prototype, ionic wind, arrays

I. Introduction

Ionic wind is created from the momentum transfer between the ions produced by a discharge and the surrounding neutral molecules. Ionic wind research has a long history, as reported in [1]–[3]. Methods for generating ionic wind can be divided into two discharge types: a DC corona discharge and an AC dielectric barrier discharge (AC DBD). Recently, the term plasma actuator has become more commonly used for AC DBD operations [4], [5]. Furthermore, the phenomenon of ionic wind is now known as the electrohydrodynamic (EHD) effect. EHD phenomena have various applications, such as EHD thrust [6], EHD flow control [4], [7], EHD drying [8], EHD cooling [9], [10], and the EHD gas pump [11], [12]. However, devices based on the EHD effect are typically prepared using conventional materials such as plastic, glass tubes/plates, ceramics, and insulating tape as well as metals for the wire, needle, or plate electrodes. When these materials are used in the preparation of EHD devices, design limitations exist that present obstacles to optimization. To overcome this problem, an additive manufacturing technology has opened the door to innovation in industrial manufacturing [13]. In particular, three-dimensional (3D) printing technologies are receiving considerable attention. To date, numerous types of items have been produced by 3D printers including tissue scaffolds [14], [15], microfluidic and pneumatic devices [16], [17], spray chambers [18], highly specialized electronics [19], [20], and musical instruments [21]. We introduced 3D printing technology to the field of plasma processing [22], by constructing a DBD plasma reactor for water treatment and then evaluated its performance in comparison with a normal reactor.

In this study, we used a low-cost 3D printer to produce ionic wind devices (IWDs). Here, we present a report on the design, construction, and operation of IWDs. Moreover, to take advantage of the rapid prototyping feature of 3D printers, we propose an array structure of IWDs that offers broad control of the air flow distribution.

Corresponding author: Seiji Kanazawa
e-mail address: skana@oita-u.ac.jp

Presented at the 3rd ISNPEDADM 2015 (New electrical technologies for environment), in October 2015

II. 3D-printed ionic wind device

Fig. 1 shows a schematic of the DC-corona-discharge-induced ionic wind device that we used as the 3D prototype model in this study. We adopted a needle-to-mesh electrode configuration, and except for metallic electrodes, all insulating parts were prepared with acrylonitrile butadiene styrene (ABS) plastic using a 3D printer (Value 3D MagiX MF-1000, Mutoh Engineering, Japan) on the basis of fused-deposition modeling. Figs. 2 and 3 show the 3D computer-aided design (CAD) data for 3D printing and its prototype ionic wind device, respectively. The gap between the needle and the mesh is adjustable from 5 to 15 mm by a screw-turning mechanism, because gap distance is a key parameter for determining the ionic wind velocity. The needle electrode was made from a stainless steel needle (curvature radius of the tip = 38 μm), and the mesh electrode was 30-mesh stainless steel. The needle electrode is connected to a high-voltage dc power supply (Matsusada Precision, Inc., HAR-50R6-LF), while the mesh electrode is grounded, to generate a corona discharge. We measured the flow velocities with a hot-wire anemometer (Kanomax, Anemomaster, 6501-A0), and performed the experiment in air at atmospheric pressure and ambient temperature.

III. Results

A. Single-IWD

Fig. 4 shows the current-voltage characteristics for a positive DC corona discharge. The corona occurs at onset voltages of 4.1, 5.7, and 9.2 kV for gap distances of 6, 10, and 15 mm and the discharge current increases with applied voltage until spark transition voltages of 8.6, 13.5, and 19.1 kV, respectively. Fig. 5 shows the luminescence of the discharge. In general, a glow-type discharge appears at the tip of the needle electrode,

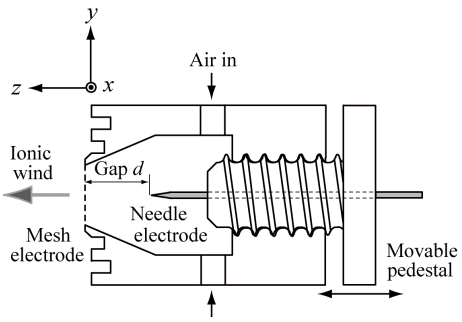

Fig. 1. Schematic of the experimental setup (single IWD).

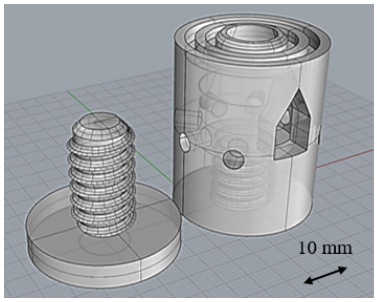

Fig. 2. 3D computer-aided design (CAD) data for single-IWD.

Fig. 3. 3D-printed single-IWD with variable gap distance.

as shown in Fig. 5(a). However, under our experimental conditions, at currents greater than approximately 10 μA, a streamer-like discharge can be observed, as shown in Fig. 5(b).

Fig. 6 shows typical ionic wind characteristics. We measured the time-averaged ionic wind velocity at $x = y = 0$ and $z = 10$ mm, as defined in Fig. 1. It is well known that ionic wind velocity is proportional to the applied voltage or square root of the current [1]

$$\nu = k\sqrt{\frac{i}{\rho\mu}} \tag{1}$$

where k is a constant that depends mainly on the electrode configuration, i is the discharge current, ρ is the gas density, and μ is ion mobility. When the gap distance is less than 10 mm, the velocity changes non-monotonically with the square root of the current in the higher current region. This may be due to the discharge mode transition from glow to streamer.

Fig. 7 shows the time-averaged velocity profiles at different positions of the z-axis, where $z = 0$ corresponds to a surface

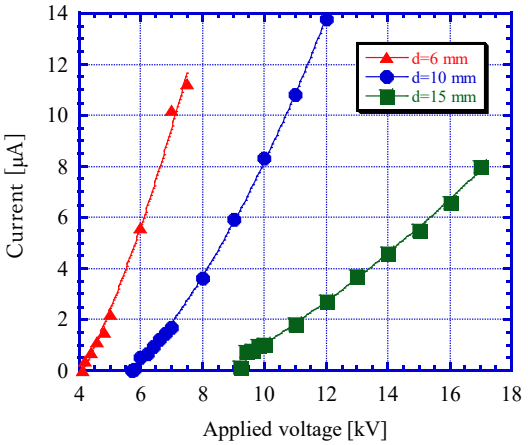

Fig. 4. Current-voltage characterisitcs for various electrode gaps.

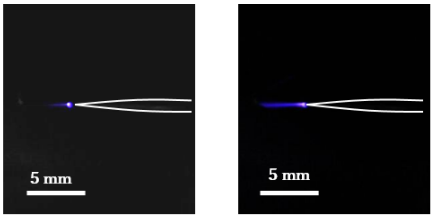

(a) 9 kV, 5.1 μA (b) 11 kV, 10.2 μA

Fig. 5. Luminescence of the discharge ($d = 10$ mm).

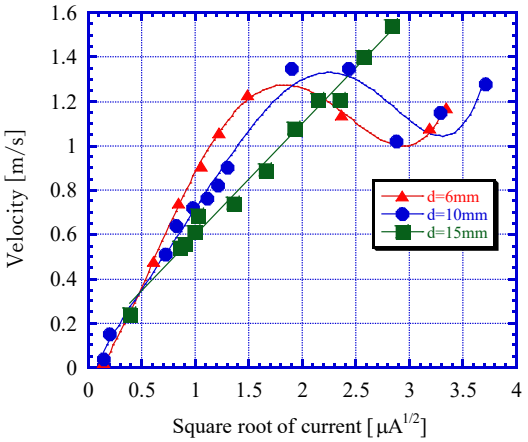

Fig. 6. Ionic wind velocity characteristics for various electrode gaps.

of the mesh electrode. In the IWD prototype shown in Fig. 3, the point of maximum velocity is deviated from the center of the IWD. This may be due to a misalignment of the needle electrode against the variable pedestal caused by a tolerance for the insertion of the needle electrode. To adjust the profiles, we attached a nozzle to the exit of the IWD. Several types of nozzles were designed, as shown in Fig. 8. Using a nozzle, more uniform profiles could be obtained, as shown in Fig. 7, and the maximum velocity increased for nozzle types B and

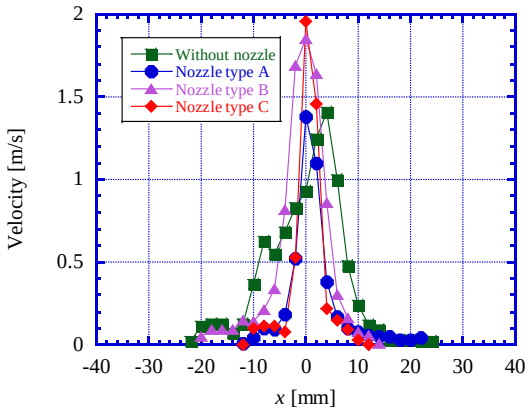

(a) $z = 20$ mm

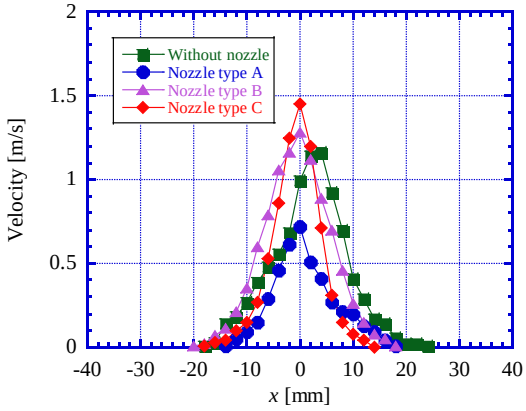

(b) $z = 40$ mm

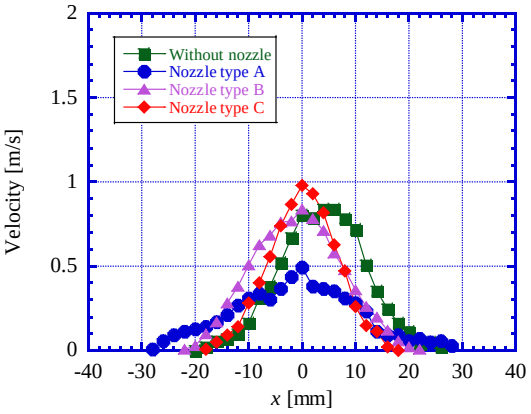

(c) $z = 60$ mm

Fig. 7. Ionic wind velocity profiles ($d = 10$ mm, $y = 0$ mm, and $V = 10$ kV).

C. Moreover, we found that as the distance from the aperture increases, the ionic wind becomes weaker and more uniform owing to greater momentum loss and the diffusion process.

Consequently, 3D-printing technology can be used to efficiently design and fabricate the IWD.

B. Three-IWD array

Fig. 9 shows a schematic of the three-IWD array in a triangular geometry. Here, we changed the shape of the IWD

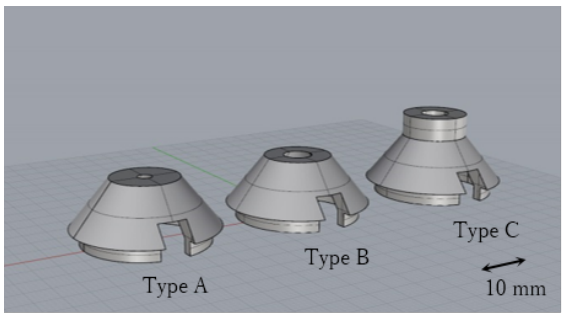

Fig. 8. Nozzles for the control of velocity profiles (Types A, B, and C have an aperture of 3, 6, and longtype 6 mm in diameter, respectively).

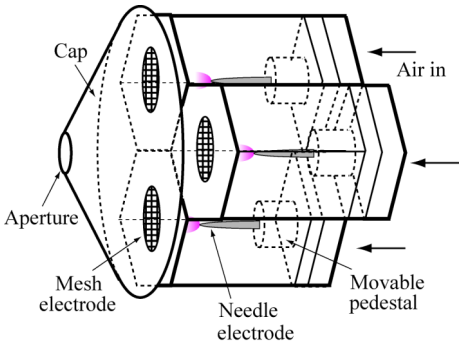

Fig. 9. Schematic of the three-IWD array arranged in a triangular geometry with a cap.

structure from cylindrical to hexagonal. Each IWD is mounted in a 3D-printed ABS case, with each IWD compartment having one power supply. A cap with an aperture 10 mm in diameter is attached on the IWD-housing case. Fig. 10 shows photos of the 3D-printed parts for the three-IWD array. Fig. 11 shows the dependence of the ionic wind velocity on the square root of the current. For comparison, we operated a single-IWD without a nozzle to retain the same aperture diameter with the three-IWD array. We measured the time-averaged ionic wind velocity at $x = y = 0$ and $z = 55$ mm. The ionic wind velocity characteristics of the three-IWD array were generally similar to those of the single-IWD. However, in the case of the IWD array, a higher ionic wind velocity can be obtained when operating at a higher square root of the current (i.e., greater than 3 $\mu A^{1/2}$). This is due to the superposition of three corona discharges in an array system with a front cap. Fig. 12 shows time-averaged velocity profiles for the single-IWD and three-IWD array at $z = 55$ mm. Since both devices were operated at the same applied voltage of 13 kV, the discharge current of the three-IWD array is approximately three times higher than that of the single-IWD, resulting in different velocity profiles. Consequently, we can broadly control ionic wind velocity and its profile using an array configuration. In an array system, a precise adjustment of the discharge gap distance between the needle and mesh electrodes for each discharge device is necessary to obtain a more uniform air flow distribution if a front cap is not installed.

Fig. 13 shows a three-IWD array with a linear geometry. The left- and right-hand devices can be tilted toward the center

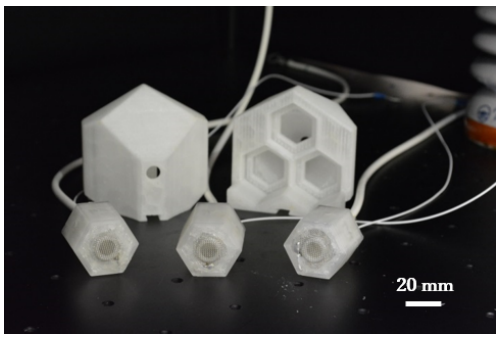

Fig. 10. 3D-printed parts for a three-IWD array in a triangular geometry. Front: a single-IWD with a hexagonal shape Backward: front side (left) and back side (right) of the case.

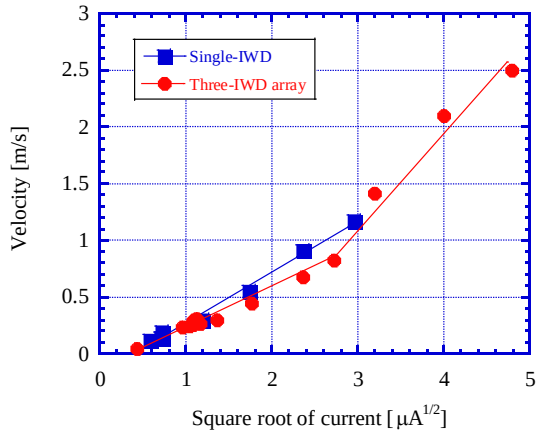

Fig. 11. Comparison of ionic wind velocity characteristics between a single-IWD and a three-IWD array ($d = 15$ mm and $z = 55$ mm).

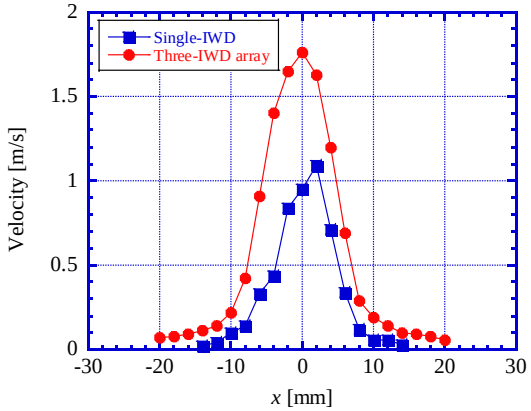

Fig. 12. Comparison of ionic wind velocity profiles between a single-IWD and a three-IWD array ($d = 15$ mm, $y = 0$ mm, $z = 55$ mm, and $V = 13$ kV).

device. As one application of this IWD array, we investigated EHD cooling, as shown in Fig. 14. In this experiment, we used a heat plate in the EHD cooling test. The plate was spray-painted black to maintain a known emissivity of 0.95 and was heated from the rear side using a soldering iron. The surface temperature was measured with an infrared (IR) camera (FLIR C2). Furthermore, K-type thermocouples were

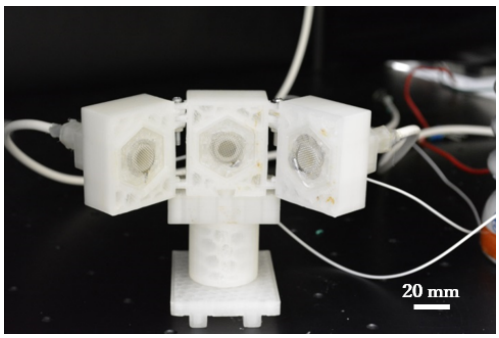

Fig. 13. 3D-printed three-IWD array with linear geometry. In this photo, the left and right devices are tilted at 45° angle toward the center device.

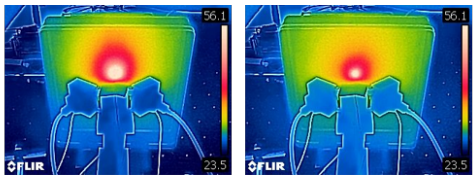

(a) before discharge (b) after discharge

Fig. 14. IR images of EHD cooling using a three-IWD array ($d = 15$ mm and $V = -15$ kV)

attached on the surface of the plate near the center area to ensure accuracy of the IR monitoring. The ionic wind was generated by negative corona discharge because of its higher spark transition. Figs. 14(a) and (b) show the IR images before and during EHD cooling, respectively. A significant cooling enhancement occurs around the heating point. For our experimental conditions, the observed maximum temperature decrease was 35°C. We therefore confirm that the 3D-printed IWD operates in a stable manner and compares favorably with the conventional IWD prepared using normal materials.

IV. Conclusion

3D printing technology has opened a new door for the design and fabrication of a prototype ionic wind device using a corona discharge. This technology offers a variable, fast, and cost-efficient production process for the development of prototype devices. In this study, we designed a novel EHD system with a multi-device array configuration. We verified the feasibility of this approach and evaluated the performance of the IWDs developed with this technology.

References

[1] M. Robinson, "Movement of air in the electric wind of the corona discharge," *Transactions of the American Institute of Electrical Engineers, Part I: Communication and Electronics*, vol. 80, pp. 143–150, 1961.

[2] T. Adachi, H. Yamashita, H. Nakabayashi, and C. Masada, "The comparative characteristics of five types of ionic wind (in Japanese)," *Memoirs of the Faculty of Engineering, Yamaguchi University*, vol. 27, pp. p105–112, 1976.

[3] E. D. Fylladitakis, M. P. Theodoridis, and A. X. Moronis, "Review on the history, research, and applications of electrohydrodynamics," *IEEE Transactions on Plasma Science*, vol. 42, pp. 358–375, 2014.

[4] E. Moreau, "Airflow control by non-thermal plasma actuators," *Journal of Physics D: Applied Physics*, vol. 40, pp. 605–636, 2007.

[5] G. Touchard, "Plasma actuators for aeronautics applications -state of art review-," *International Journal of Plasma Environmental Science and Technology*, vol. 2, pp. 1–25, 2008.
[6] E. A. Christenson and P. S. Moller, "Ion-neutral propulsion in atmospheric media," *AIAA Journal*, vol. 5, pp. 1768–1773, 1967.
[7] J. Reece Roth, D. M. Sherman, and S. P. Wilkinson, "Boundary layer flow control with a one atmosphere uniform glow discharge surface plasma," in *Proceedings of the 36th AIAA Aerospace Sciences Meeting and Exhibit*, Reno, NV, 1998, AIAA 98-0328.
[8] T. R. Bajgai, G. S. V. Raghavan, F. Hashinaga, and M. O. Ngadi, "Electrohydrodynamic drying - A concise overview," *Drying Technology*, vol. 24, pp. 905–910, 2006.
[9] D. B. Go, S. V. Garimella, T. S. Fisher, and R. K. Mongia, "Ionic winds for locally enhanced cooling," *Journal of Applied Physics*, vol. 102, p. 053302, 2007.
[10] R.-T. Huang, W.-J. Sheu, and C.-C. Wang, "Heat transfer enhancement by needle-arrayed electrodes - An EHD integrated cooling system," *Energy Conversion and Management*, vol. 50, pp. 1789–1796, 2009.
[11] J.-S. Chang, H. Tsubone, G. D. Harvel, and K. Urashima, "Narrow-flow-channel-driven ehd gas pump for an advanced thermal management of microelectronics," *IEEE Transactions on Industry Applications*, vol. 46, pp. 1151–1158, 2010.
[12] N. Takeuchi and K. Yasuoka, "Efficiency of a wire-rod type electrohydrodynamic gas pump under negative corona operation," *IEEE Transactions on Plasma Science*, vol. 37, pp. 1021–1026, 2009.
[13] C. Anderson, *Makers: The New Industrial Revolution (in Japanese)*. NHK Publishing Co., 2012.
[14] G. Villar, A. D. Graham, and H. Bayley, "A tissue-like printed material," *Science*, vol. 340, pp. 48–52, 2013.
[15] F. F. Yan, Y. Y. Liu, H. P. Chen, F. H. Zhang, L. L. Zheng, and Q. X. Hu, "A multi-scale controlled tissue engineering scaffold prepared by 3D printing and NFES technology," *AIP Advances*, vol. 4, p. 031321, 2014.
[16] A. Bonyar, H. Santha, M. Varga, B. Ring, A. Vitez, and G. Harsanyi, "Characterization of rapid PDMS casting technique utilizing molding forms fabricated by 3D rapid prototyping technology (RPT)," *International Journal of Material Forming*, vol. 7, pp. 189–196, 2014.
[17] V. Dragone, V. Sans, M. H. Rosnes, P. J. Kitson, and L. Cronin, "3d-printed devices for continuous-flow organic chemistry," *Beilstein Journal of Organic Chemistry*, vol. 9, pp. 951–959, 2013.
[18] D. F. Thompson, "Rapid production of cyclonic spray chambers for inductively coupled plasma applications using low cost 3D printer technology," *Journal of Analytical Atomic Spectrometry*, vol. 29, pp. 2262–2266, 2014.
[19] S. J. Leigh, R. J. Bradley, C. P. Purssell, D. R. Billson, and D. A. Hutchins, "A simple, low-cost conductive composite material for 3D printing of electronic sensors," *PLoS ONE*, vol. 7, p. e49365, 2012.
[20] K. Sun, T. S. Wei, B. Y. Ahn, J. Y. Seo, S. J. Dillon, and J. A. Lewis, "3D printing of interdigitated Li-ion microbattery architectures," *Advanced Materials*, vol. 25, pp. 4539–4543, 2013.
[21] A. Zoran, "The 3D printed flute: Digital fabrication and design of musical instruments," *Journal of New Music Research*, vol. 40, pp. 379–387, 2011.
[22] S. Kanazawa, K. Eto, W. Imagawa, S. Akamine, and R. Ichiki, "3D-printed atmospheric-pressure plasma reactors," *International Journal of Plasma Environmental Science and Technology*, vol. 9, pp. 103–106, 2015.